Statistical Neighbor Distance Influence in Active Contours

Jing Yang[1], Lawrence H. Staib[1], and James S. Duncan[1]

Yale University, P.O. Box208042, New Haven CT 06520-8042, USA
{j.yang,lawrence.staib,james.duncan}@yale.edu

Abstract. In this paper, we propose a new model for segmentation of images containing multiple objects. In order to take advantage of the constraining information provided by neighboring objects, we incorporate information about the relative position and shape of neighbors into the segmentation process by defining a new "distance" term into the energy functional. We introduce a representation for relative neighbor distances, and define a probability distribution over the variances of the relative neighbor distances of a set of training images. By minimizing the energy functional, we formulate the model in terms of level set functions, and compute the associated Euler-Lagrange equations. The contours evolve both according to the relative distance information and the image grey level information. Several objects in an image can be automatically detected simultaneously.

1 Introduction

Medical image segmentation is an important and challenging problem and a necessary first step in many image analysis and quantitation methods. Sophisticated automated and semi-automated techniques are required.

Since the original work by Kass et al. (1987) [1], extensive research has been done on active contour models or "snakes", where an initial contour is deformed towards the boundary of the object to be detected by minimizing an energy functional.

In the problem of curve evolution, level set methods [2] have been used extensively, because they allow for automatic changes in the topology. Novel geometric models of active contours have been proposed based on curve evolution and geometric flows [4] [5] [6]. By using the level-sets based numerical algorithm, several objects can be segmented simultaneously.

Recently, Chan and Vese [3] have proposed an active contour model, based on techniques of curve evolution, using a Mumford-Shah functional for segmentation with a level sets. In the level set formulation, the problem becomes a "mean-curvature flow". This model can detect objects whose boundaries are not necessarily defined by gradient.

The idea of incorporating prior information into image segmentation has received a large amount of attention in recent years and has been approached

T. Dohi and R. Kikinis (Eds.): MICCAI 2002, LNCS 2488, pp. 588–595, 2002.

using point distribution models (Cootes,et al.)[7], Fourier parameters (Staib and Duncan)[8], and statistical shape inforamtion (Leventon et al.)[9].

In many cases, objects to be detected have one or more neighboring structures which have a consistent location and shape that provides a configuration and context that aids in the delineation. The relative positions or distances among these neighbors can also be modeled based on statistical information from a training set. Though applicable in many domains these models are particularly useful for medical applications. For example, the anatomical structures that appear in magnetic resonance (MR) or computed tomography (CT) scans are often segmented for use in surgical planning, navigation, simulation, diagnosis and therapy evaluation. Without a prior model to constrain the segmentation, the algorithms often fail due to difficult challenges such as poor image contrast, noise, and missing or diffuse boundaries. It can be made easier if suitable models of the relative distances among neighboring structures are available.

We incorporate relative position and shape information of neighbors by defining a new "distance" term into the energy functional. We introduce the representation for relative neighbor distances, and define a probability distribution over a training set. By minimizing the energy functional, we formulate the model in terms of level set functions, and compute the associated Euler-Lagrange equations. The contours evolve both according to the relative distance information and the image grey level information.

2 Probability Distribution of Neighbor Distances

2.1 Binary Shape Alignment

Consider a training set of N images, with M objects or structures in each image. Let the training set consist of a set of MN binary images $\{I_i^n | i = 1, 2, ...M; n = 1, 2, ..., N\}$, each with values one inside and zero outside object i. To compute the relative distances in the training set, we first transform each binary image, I_i^n, into another binary image $I_j^n, j \neq i$ to jointly align them with a similarity transformation. The idea is to calculate the set of transformation matrices $\{T_{ij}^n | i, j = 1, 2, ...M \cap j \neq i\}$, where T_{ij}^n transforms the coordinates of I_i^n into the coordinates of $I_j^n, j \neq i$. T_{ij}^n consists of translation, scale and axis rotations. In 2D, the transformed binary image $\tilde{I}_{ij}^n$ is defined as: $\tilde{I}_{ij}^n = I_i^n(T_{ij}^n \cdot [x, y, 1]^T)$

An effective way to calculate T_{ij}^n is to descend along the energy functional:

$$E_{ij\,align}^n = \frac{\int_\Omega (\tilde{I}_{ij}^n - I_j^n)^2 dA}{\int_\Omega (\tilde{I}_{ij}^n + I_j^n)^2 dA} \tag{1}$$

Where Ω denotes the image domain. By minimizing (1), we minimize the difference between $\tilde{I}_{ij}^n$ and I_j^n[10]. To illustrate, Figure 1 shows two neighboring objects where the dotted curves are the aligned versions of the two boundaries.

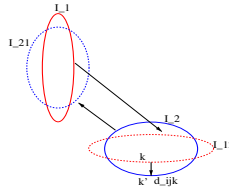

Fig. 1. Shape alignments of 2 objects and neighbor distance definition.

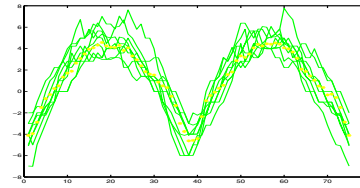

Fig. 2. Relative distance distribution of the two shapes in Figure 3a.

2.2 Neighbor Distances Definition

We define d^n_{ijk} as the nearest distance of the k th point on the boundary of object i in $\tilde{I}^n_{ij}$ to object j in I^n_j along $\pm\boldsymbol{n}$, where $\boldsymbol{n}$ is the normal direction at the k th point of object i, as shown in Figure 1. The training set, D, consists of a set distance matrices $D = \{D^1, D^2, ..., D^N\}$, where $D^n = \{d^n_{ijk} | i, j = 1, 2, ..., M; k = 1, 2, ..., K\}$ is the distance matrix of the n th image in the training set. Note that d^n_{ijk} is not necessarily equal to $d^n_{jik'}$ because the optimal transformation may differ. Our goal is to build a statistical model over this distribution of distance matrices, under a Gaussian assumption $N(\bar{d}_{ijk}, \sigma_{ijk})$. $\bar{d}_{ijk}$ and σ^2_{ijk} are the mean and variance of d^n_{ijk}. Figure 3 shows the outlines of two objects in a training set with 9 images. The computed relative distance matrices D of the training set in Figure 3 are shown in Figure 2. The yellow '*' curve is the mean relative distance between the two shapes.

3 Description of the Model

3.1 Energy Functional

Our method defines the segmentation problem in terms of minimizing an energy functional. Given the distribution of the relative neighbor distances, the prior information about the relative positions of all the objects of interest in an image can be modeled as an energy term. The corresponding term in the level set evolution equation of the model pulls the surface in the direction such that d_{ijk} approaches its maximum likelihood estimation $\hat{d}_{ijk}$ in the final segmentation.

Assume C_i is the evolving curve corresponding to object i in Ω, C_{i0} is the boundary of object i. Now, let us consider the following energy terms:

$$E_{ineighbor} = \sum_{j=1, j\neq i}^{M} \int_{C_i} [d_{ij}(x,y) - \hat{d}_{i,j}(x,y)]^2 dxdy \ , \ E_{neighbor} = \sum_{i=1}^{M} E_{ineighbor} \tag{2}$$

It is obvious that C_{i0}, the boundary of object i, is the minimizer of $E_{ineighbor}$. Boundary $C_0 = \{C_{i0} | i = 1, 2, ..., M\}$ of the M objects of interest is the minimizer of $E_{neighbor}$. In our active contour model, we will minimize the energy term

$E_{neighbor}$ and we will add image gray level information based energy terms and regularizing terms, like the length of the curve C_i and (or) the area of the region inside C_i. Here, we use the energy terms defined by Chan [3] as the gray level information based energy terms. Therefore, we introduce the energy functional of each object of interest i as $E_i(c_{1i}, c_{2i}, C_i)$, defined by:

$$\begin{aligned} E_i(c_{1i}, c_{2i}, C_i) &= E_{ineighbor} + E_{ilength} + E_{iarea} + E_{iimage} \\ &= \sum_{j=1, j\neq i}^{M} w_{ij} \int_{C_i} [d_{ij}(x,y) - \hat{d}_{i,j}(x,y)]^2 dxdy \\ &\quad + \mu_i \cdot Length(C_i) + \nu_i \cdot Area(inside(C_i)) \\ &\quad + \lambda_{1i} \int_{inside(C_i)} |I(x,y) - c_{1i}|^2 dxdy \\ &\quad + \lambda_{2i} \int_{outside(C_i)} |I(x,y) - c_{2i}|^2 dxdy \end{aligned} \tag{3}$$

Where w_{ij}, μ_i, ν_i, λ_{1i}, and λ_{2i} are non-negative fixed parameters. I is the image. C_i is the evolving curve of object i, and the constants c_{1i}, c_{2i}, depending on C_i, are the averages of I inside C_i and respectively outside C_i. We wish to minimize the total energy of all the objects of interest in the image $E_{total}(c_1, c_2, C)$:

$$\min_{c_1, c_2, C} E_{total}(c_1, c_2, C) = \min_{c_1, c_2, C} \sum_{i=1}^{M} E_i(c_{1i}, c_{2i}, C_i) \tag{4}$$

Where $C = \{C_i | i = 1, 2, ...M\}$, $c_1 = \{c_{1i} | i = 1, 2, ...M\}$, $c_2 = \{c_{2i} | i = 1, 2, ...M\}$. This minimization problem can be formulated and solved using the level set method. In this way, we can realize the segmentation of multiple objects simultaneously.

3.2 Estimation of Relative Neighbor Distances

In the functional $E_{total}(c_1, c_2, C)$, we include terms that incorporate information of the relative neighbor distances of the objects being segmented. For each given evolving curve C_i, we seek the maximum likelihood estimate of the relative neighbor distances d_{ijk} of the final curve:

$$\hat{d}_{ijk} = \arg\max_{\hat{d}_{ijk}} p(\tilde{d}_{ijk}/d_{ijk}) = \arg\max_{\hat{d}_{ijk}} \frac{p(d_{ijk}/\tilde{d}_{ijk}) p(\tilde{d}_{ijk})}{p(d_{ijk})} \tag{5}$$

The first term in the numerator computes the probability of the relative neighbor distance among certain evolving curves given the relative neighbor distances among the final curves. It is reasonable to model this term as a Gaussian function: $N(\tilde{d}_{ijk}, \sigma_{ijk})$. The second term in the numerator of (5) is based on our prior models, as described in section 2.2. Finally, we discard the normalization term in the denominator of (5) as it does not depend on $\tilde{d}_{ijk}$.

3.3 Level Set Formulation of the Model

In the level set method, C_i is the zero level set of a higher dimensional surface Ψ_i corresponding to the i th object being segmented, i.e., $C_i = \{(x,y) | \Psi_i(x,y) = 0\}$.

The evolution of the curve C_i is given by the zero-level curve at time t of the function $\Psi_i(t,x,y)$. We define that Ψ_i is positive outside C_i and negative inside C_i. Each of the M objects being segmented in the image has its own C_i and Ψ_i. Thus, we have M level set functions.

For the level set formulation of our model, we replace C with Ψ in the energy functional in (3) using regularized versions of the Heaviside function H and the Dirac function δ [3], denoted by H_ε and δ_ε:

$$\begin{aligned} E_i(c_{1i},c_{2i},C_i) = &\sum_{j=1,j\neq i}^{M} w_{ij}\int_\Omega [d_{ij}(x,y)-\hat{d}_{i,j}(x,y)]^2\delta_\varepsilon(\Psi_i(x,y))|\nabla\Psi_i(x,y)|dxdy \\ &+\mu_i\int_\Omega \delta_\varepsilon(\Psi_i(x,y))|\nabla\Psi_i(x,y)|dxdy+\nu_i\int_\Omega(1-H_\varepsilon(\Psi_i(x,y)))dxdy \\ &+\lambda_{1i}\int_\Omega |I(x,y)-c_{1i}|^2(1-H_\varepsilon(\Psi_i(x,y)))dxdy \\ &+\lambda_{2i}\int_\Omega |I(x,y)-c_{2i}|^2 H_\varepsilon(\Psi_i(x,y))dxdy \end{aligned} \tag{6}$$

To compute the associate Euler-Lagrange equation for each unknown level set function Ψ_i, we keep c_{1i} and c_{2i} fixed, and minimize E_{total} with respect to $\Psi_i (i=1,2,...M)$ respectively. Parameterizing the descent direction by artificial time $t\geq 0$, the equation in $\Psi_i(t,x,y)$ is:

$$\begin{aligned} \frac{\partial\Psi_i}{\partial t} = &\delta_\varepsilon(\Psi_i)\cdot div[\frac{\nabla\Psi_i}{|\nabla\Psi_i|}]\sum_{j=1,j\neq i}^{M} w_{ij}[d_{ij}(x,y)-\hat{d}_{ij}(x,y)]^2 \\ &+\sum_{j=1,j\neq i}^{M} 2w_{ji}\delta_\varepsilon(\Psi_j)\cdot|\nabla\Psi_j|[d_{ji}(x,y)-\hat{d}_{ji}(x,y)] \\ &+\delta_\varepsilon(\Psi_i)[\mu_i\cdot div[\frac{\nabla\Psi_i}{|\nabla\Psi_i|}]+\nu_i+\lambda_{1i}|I(x,y)-c_{1i}|^2-\lambda_{2i}|I(x,y)-c_{2i}|^2] \end{aligned} \tag{7}$$

3.4 Evolving the Surface

We approximate H_ε and δ_ε as follows [3]:$H_\varepsilon(z)=\frac{1}{2}[1+\frac{2}{\pi}\arctan(\frac{z}{\varepsilon})]$, $\delta_\varepsilon(z)=\frac{\varepsilon}{\pi(\varepsilon^2+z^2)}$. c_{1i} and c_{2i} are defined by: $c_{1i}(\Psi_i)=\frac{\int_\Omega I(x,y)\cdot(1-H(\Psi_i(x,y)))dxdy}{\int_\Omega(1-H(\Psi_i(x,y)))dxdy}$, $c_{2i}(\Psi_i)=\frac{\int_\Omega I(x,y)\cdot H(\Psi_i(x,y))dxdy}{\int_\Omega H(\Psi_i(x,y))dxdy}$.

Given the surfaces $\Psi_i(i=1,2,...M)$ at time t, we seek to compute evolution steps that bring all the zero level set curves to the correct final segmentation based on the prior relative distance information and image information. At each stage of the algorithm, we recompute the relative distances d_{ij} and estimation $\hat{d}_{ij}$ as well as the constants c_{1i} and c_{2i}. We then update the Ψ_i. This is repeated until convergence.

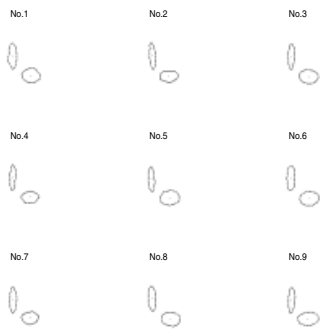

Fig. 3. Training set: Outlines of 2 shapes in 9 images.

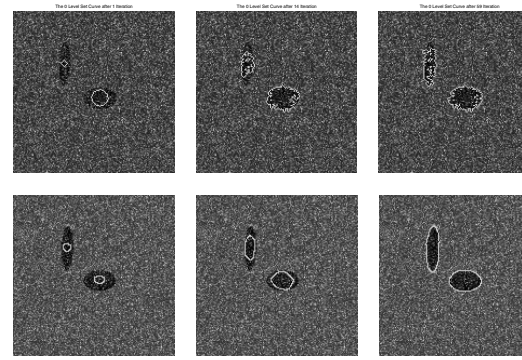

Fig. 4. Initial, middle, and final steps in the segmentation of two shapes in a synthetic image.

The parameters w_{ij}, μ_i, ν_i, λ_{1i}, and λ_{2i} are used to balance the influence of the relative distance information model and the image information model. The tradeoff between relative distance and image information depends on how much faith one has in the distance model and the imagery for a given application. We set these parameters empirically for particular segmentation tasks, given the general image quality and the prior relative distance information.

4 Experimental Results

We have used our model on various synthetic and real images, with at least two different types of contours and shapes. We have generated a training set of synthetic images of two elliptic objects with the addition of Gaussian noise, as shown in Figure3. Figure 2 shows the distance distribution. Figure 4 illustrates several steps in the segmentation of two synthetic objects in a noisy image. The result of using neighbor information (lower row) is much better than only use the image grey level information (upper row).

Figure 5 shows the construction of a two object model (left ventricle and right ventricle) from 2D MRI heart images. In Figure 6, we show an example delineation of the ventricles with the initial, middle, and final steps in the curve evolution process. The experiment was first performed without using neighbor distance information, as shown in Figure 6 top. The evolving curves stopped at a place where there is a bigger change of the grey level. They cannot lock onto the shape of the objects. We then use the relative distance information to segment the same image again, as shown in Figure 6 bottom. By taking the statistical relative distance information of the two shapes from the training set shown in Figure 5, the curves are able to converge on the desired boundaries even though some parts of the boundaries are too blurred to be detected using only grey level information. Both of the segmentations converged in several minutes on an SGI Octane with a 255MHz R10000 processor.

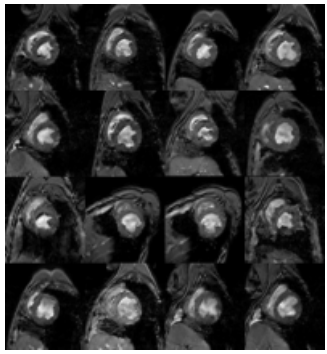

Fig. 5. Training set: 16 MR heart images.

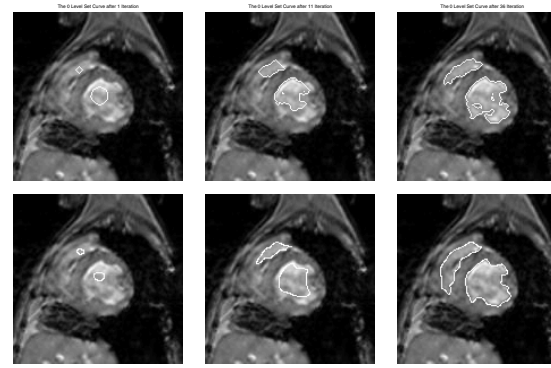

Fig. 6. Initial, middle, and final steps in the segmentation of two shapes in a heart image.

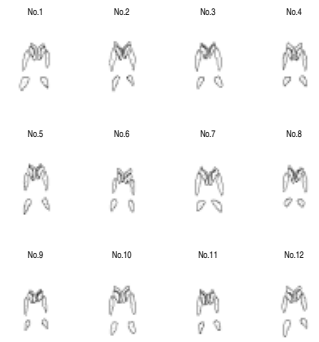

Fig. 7. Training set: outlines of 8 shapes in 12 MR brain images.

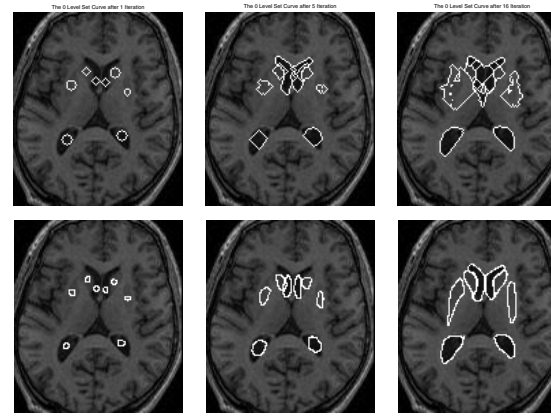

Fig. 8. Initial, middle, and final steps in the segmentation of 8 shapes in a brain image.

In Figure 8, we show that our model can detect multiple objects of different intensities, and with blurred boundaries in a 2D MR brain image. Figure 8 top shows the result of using the model based only on grey level information. The lower (posterior) portions of the lateral ventricles can be segmented perfectly since they have clearer boundaries. But for the other six structures, their boundaries are so blurred that they cannot be detected using grey level information alone. To incorporate neighbor information, we used a training set as shown in Figure 7. We also ran our algorithm to segment eight different objects: the lateral ventricles, heads of the caudate nucleus, and putamen. Segmenting all eight subcortical structures took approximately twenty minutes.

To assess the segmentation results, we computed the undirected distance between the computed boundary $A(N_A$ points) and the manual boundary B: $H(A,B) = \max(h(A,B), h(B,A))$, $h(A,B) = \frac{1}{N_A} \sum_{a \in A} \min_{b \in B} \|a - b\|$.

For our experiments, we showed improvement in all the three cases comparing with/without neighbor influence: synthetic 2.1/5.3, heart 2.6/4.2, brain 2.8/9.6.

5 Conclusions

A new model for automated segmentation of images containing multiple objects by incorporating the information about the relative position and shape of neighbors in the segmentation process has been presented. Our model is based on defining a new "distance" term into the energy functional. We introduce the representation for relative neighbor distances, and define a probability distribution over the variances of the relative neighbor distances of a set of training images. By minimizing the energy functional, we formulate the model in terms of level set functions, and compute the associated Euler-Lagrange equations. The contours evolve both according to the relative distance information and the image grey level information. Multiple objects in an image can be automatically detected simultaneously. We believe that our model can also be extended to 3D image segmentation.

References

1. M. Kass, A. Witkin, D. Terzopoulos.: Snakes: Active contour models. Int'l Journal on Computer Vision, **1** (1987) 321–331
2. S. Osher and J. A. Sethian.: Fronts propagating with curvature-dependent speed: Algorithms based on Hamilton-Jacobi Formulation. J. Comp. Phy. **79** (1988) 12–49
3. T. Chan, L. Vese.: Active Contours Without Edges. IEEE Transactions on Image Processing, vol.**10** No. **2** (2001) 266–277
4. V. Caselles, F. Catte, T. Coll, and F. Dibos.: A geometric model for active contours in image processing. Numer. Math. **66** (1993) 1–31
5. V. Caselles, R. Kimmel, and G. Sapiro.: Geodesic active contours. Int. J. Comput. Vis. vol.**22** No. **1** (1997) 61–79
6. R. Malladi, J. A. Sethian, and B. C. Vemuri.: A topology independent shape modeling scheme. Proc. SPIE Conf. Geometric Methods Computer Vision II, vol.**2031** (1993) 246–258
7. T. Cootes, C. Beeston, G. Edwards, and T. Taylor.: Unified framework for atlas matching using active appearance models. Information Processing in Medical Imaging, (1999)
8. L.Staib, J. Duncan.: Boundary finding with parametrically deformable models. PAMI, **14**(11) (1992) 1061–1075
9. M. Leventon, E. Grimson, and O. Faugeras.: Statistical shape influence in geodesic active contours. IEEE Conf. on Comp. Vision and Patt. Recog. **1** (2000) 316–323
10. A. Tsai, A. Yezzi, et al.: Model-based curve evolution technique for image segmentation. IEEE Conf. on Comp. Vision and Patt. Recog. vol.**1** (2001) 463–468